(4)

AFGL-TR-88-0152

REMOTE SOUNDING OF ATMOSPHERIC TEMPERATURE PROFILES USING THE DIFFERENTIAL INVERSION METHOD

Kuo-Nan Liou
Szu-Cheng S. Ou

Center for Atmospheric and Remote Sounding Studies
Department of Meteorology
University of Utah
Salt Lake City, Utah 84112

Final Report
1 May 1987 - 30 April 1988

15 June 1988

Approved for public release; distribution unlimited

AIR FORCE GEOPHYSICS LABORATORY
AIR FORCE SYSTEMS COMMAND
UNITED STATES AIR FORCE
HANSCOM AFB, MASSACHUSETTS 01731

Unclassified

SECURITY CLASSIFICATION OF THIS PAGE

REPORT DOCUMENTATION PAGE

1a. REPORT SECURITY CLASSIFICATION: Unclassified	1b. RESTRICTIVE MARKINGS
2a. SECURITY CLASSIFICATION AUTHORITY	3. DISTRIBUTION/AVAILABILITY OF REPORT: Approved for public release; distribution unlimited
2b. DECLASSIFICATION/DOWNGRADING SCHEDULE	
4. PERFORMING ORGANIZATION REPORT NUMBER(S)	5. MONITORING ORGANIZATION REPORT NUMBER(S): AFGL-TR-88- 0152
6a. NAME OF PERFORMING ORGANIZATION: Center for Atmospheric and Remote Sounding Studies; 6b. OFFICE SYMBOL (If applicable): CARSS	7a. NAME OF MONITORING ORGANIZATION: Air Force Geophysics Laboratory
6c. ADDRESS (City, State and ZIP Code): Department of Meteorology, University of Utah, Salt Lake City, Utah 84112	7b. ADDRESS (City, State and ZIP Code): Hanscom Air Force Base, Massachusetts 01731
8a. NAME OF FUNDING/SPONSORING ORGANIZATION; 8b. OFFICE SYMBOL (If applicable)	9. PROCUREMENT INSTRUMENT IDENTIFICATION NUMBER: F19628-87-K-0042
8c. ADDRESS (City, State and ZIP Code)	10. SOURCE OF FUNDING NOS.

PROGRAM ELEMENT NO.	PROJECT NO.	TASK NO.	WORK UNIT NO.
61101F	ILIR	ILIR7D	ILIR7DAA

11. TITLE (Include Security Classification): Remote Sounding of Atmospheric Temperature Profiles (Cont.)

12. PERSONAL AUTHOR(S): Kuo-Nan Liou; Szu-Cheng Ou

13a. TYPE OF REPORT	13b. TIME COVERED	14. DATE OF REPORT (Yr., Mo., Day)	15. PAGE COUNT
Final	FROM 5/1/87 TO 4/30/88	15 June 1988	52

16. SUPPLEMENTARY NOTATION: This research was supported by the AF In-house Laboratory Independent Research Fund

17. COSATI CODES			18. SUBJECT TERMS (Continue on reverse if necessary and identify by block number)
FIELD	GROUP	SUB GR.	Remote Sensing, inversion Theory, Differential Inversion Method, HIRS, Temperature Retrieval, K-Correlated Method, Error Analysis

19. ABSTRACT (Continue on reverse if necessary and identify by block number)

The differential inversion method (DIM) is presented in the context of the fundamental principles governing the transfer of radiation for plane-parallel atmospheres in local thermodynamic equilibrium. In the Laplace inverse plane, the Planck intensity is linearly related to upwelling radiances weighted by the weighting function. By applying the inverse transform, the local Planck intensity can be exactly expressed by a linear combination of the derivatives of upwelling radiances in the logarithmic pressure coordinate. Using seven HIRS channels, numerical analyses of the DIM for temperature retrievals are carried out. Results based on distinct U.S. standard and tropical profiles show that the DIM converges to the true temperature solution with an accuracy of 1-2 K for tropospheric temperatures using a fifth-order polynomial function to fit seven HIRS radiances. The

20. DISTRIBUTION/AVAILABILITY OF ABSTRACT	21. ABSTRACT SECURITY CLASSIFICATION
UNCLASSIFIED/UNLIMITED ☒ SAME AS RPT ☐ DTIC USERS ☐	Unclassified

22a. NAME OF RESPONSIBLE INDIVIDUAL	22b. TELEPHONE NUMBER (Include Area Code)	22c. OFFICE SYMBOL
Jean J.F. King	617-377-2977	LY

DD FORM 1473, 83 APR — EDITION OF 1 JAN 73 IS OBSOLETE.

Unclassified

SECURITY CLASSIFICATION OF THIS PA

Continuation of Block 19:

DIM appears to be an efficient and powerful retrieval method for temperatures. It is free from the need for a priori data basing and requires no constraints in the retrieval. Finally, it is pointed out that the key to the success of the DIM for practical applications appears to depend on whether an appropriate curve-fitting program can be developed for observed radiances.

Continuation of Block 11:

Using the Differential Inversion Method

TABLE OF CONTENTS

Section 1

INTRODUCTION

The retrieval of atmospheric temperature and moisture profiles has been routinely performed using data from orbiting meteorological satellites in the past 15 years. However, the techniques and procedures used in the retrieval were mostly statistical in nature and were not based on the principles of radiative transfer. The solution of the radiative transfer equation for the Planck function distribution given a set of upwelling radiances at the top of the atmosphere is governed by a Fredholm equation of the first kind. This equation is known to be mathematically ill-conditioned because of the instability introduced by the inverse operation.

In most retrieval approaches, certain a priori assumptions or constraints must be imposed on the temperature profiles to be retrieved. For example, in the constrained linear inversion method developed by Twomey (1963), a mean temperature profile is first assumed. Subsequently, the retrieved temperatures are obtained using a least-square method with quadratic constraints. In the statistical method (Liou, 1980), the difference between the predicted and climatological mean temperature profiles is assumed to be a linear combination of the deviation of measured radiances from the mean for all sounding channels. In the Backus-Gilbert inversion method (Conrath, 1972), certain assumptions are imposed on the shape of the kernel function. In other numerical methods (Chahine, 1970; Smith,

1970), a simple relationship between the measured radiances and temperatures is assumed.

In an attempt to break away from the conventional techniques involving profile fitting with prechosen sets and regression methods based on statistics, King (1985) proposed a novel approach to solve the temperature inversion problem. Unlike the above-mentioned methods, the approach, referred to as the differential inversion method (DIM), directly solves for temperatures at a number of pressure levels that correspond to the peaks of the weighting function. The DIM is an exact method for the inversion of the temperature profile, in which the local Planck Intensity can be exactly expressed by a linear combination of the derivatives of upwelling radiances in the logarithmic pressure coordinate. The method is free from the need for a priori data basing and the inversion requires no constraints.

In this report, we explore the generalization and practicality of the DIM for temperature retrievals. In Section 2, we describe the fundamentals of the DIM. In Section 3, applications of this method to synthetic temperature retrievals using HIRS channels are illustrated. Finally, conclusions are given in Section 4.

Section 2

THE PHYSICAL FUNDAMENTALS OF THE DIFFERENTIAL INVERSION METHOD

2.1 Forward Radiative Transfer Equation

The upwelling radiance at the top of the atmosphere, R_ν, for a given channel may be derived from the basic radiative transfer equation for a plane-parallel atmosphere under local thermodynamic equilibrium. In the pressure coordinate, we have

$$R_\nu = B_\nu(T_S)\, T_\nu(p_S) + \int_{p_S}^{0} B_\nu(p)\, \frac{\partial T_\nu(p)}{\partial p}\, dp \ , \qquad (2.1)$$

where B_ν is the Planck intensity at wavenumber ν, T_ν the transmittance, p_S the surface pressure, and T_S the surface temperature. The first and second terms represent surface and atmospheric emission contributions, respectively.

The layer below the surface may be viewed as an infinite isothermal emitter with a temperature T_S. Thus, the surface emission contribution to the radiance R_ν, as represented by the first term in Eq. (2.1), may be expressed as

$$B_\nu(T_S)\, T_\nu(p_S) = \int_{\infty}^{P_S} B_\nu(p)\, \frac{\partial T_\nu(p)}{\partial p}\, dp \quad . \qquad (2.2)$$

In presenting Eq. (2.2), it is noted that $T_\nu(\infty) = 0$. Also, $B_\nu(p) = B_\nu(T_S)$ for $p_S < p < \infty$. In the band center, $T_\nu(p_S) = 0$, so that surface contribution to the randiance R_ν may be neglected. However, in the wing of a band,

$T_\nu(p_s) > 0$, the surface emission could be an important source for the upwelling radiance. In either case, we may substitute Eq. (2.2) into Eq. (2.1) to obtain

$$R_\nu = \int_\infty^0 B_\nu(p) \frac{\partial T_\nu(p)}{\partial p} \, dp \quad . \tag{2.3}$$

The weighting function, which signifies the weight of the Planck intensity contribution to the upwelling radiance, may be defined in the logarithm of pressure in the form

$$W_\nu(p) = - \frac{\partial T_\nu(p)}{\partial \ell n p} \quad . \tag{2.4}$$

For each wavenumber ν, the transmittance $T_\nu(p)$ decreases from 1 to 0 as the parameter $\ell n p$ increases from $-\infty$ to ∞. Hence, the weighting function is always a positive quantity, and there must be a peak value located at $p = \bar{p}$, where the rate of change of $T_\nu(p)$ reaches a maximum. The peak pressure level $\bar{p}$ varies with wavenumber ν. If ν is in the band center, $\bar{p}$ will be located at a relatively low pressure level, whereas if ν is in the wing region, $\bar{p}$ will be near the surface.

In practice, a satellite sounding instrument spans a spectral interval. The sensitivity of the instrument varies with the wavenumber, according to a response function ϕ. Assuming that there are M channels, the radiance measured by the ith channel, with response function ϕ_i, may be expressed as follows:

$$R_i = \int_0^\infty B_i(p) \, W_i(p) \, dp/p \quad , \quad i = 1,2,\ldots,M, \tag{2.5}$$

where the weighting function $W_i(p)$ is now the average of $W_\nu(p)$, defined in Eq. (2.4), weighted by the response function $\phi_i(\nu)$, viz.

$$W_i(p) = \int_{\Delta\nu_i} W_\nu(p)\ \phi_i(\nu)\ d\nu \quad , \tag{2.6}$$

with $\Delta\nu_i$ the spectral interval for the ith channel. In writing Eq. (2.5), we omit the wavenumber dependence of the Planck intensity since, over a small spectral interval, the Planck intensity does not vary significantly with frequency. Equation (2.5) is a Fredholm equation of the first kind. The conventional approach for solving this kind of equation is to assume a functional form for $B_i(p)$, and then determine the unknown coefficients in the function, based on the given distributions of R_i and W_i. In practice, since only a finite number of R_i values are available, the solution of $B_i(p)$ from the forward radiative transfer equation is mathematically ill-conditioned. However, if the integration can be removed by a proper inverse transformation, then a priori assumptions or constraints commonly added to the retrieved temperature profile will no longer be required.

2.2 Differential Inversion Method

We shall approach the inverse problem by a transformation of variables. We first define the scaled pressure $\tilde{p} = p/\bar{p}_i$. Since the weighting function $W_i(p)$ peaks at $\bar{p}_i(\tilde{p} = 1)$, we may write $W_i(\tilde{p}) = \max [W_i(p)]$. Furthermore, the following variables are introduced:

$$\begin{aligned} \bar{\pi} &= -\ \ell n\bar{p} \quad , \\ \pi &= -\ \ell np \quad , \\ v &= \bar{\pi} - \pi = \ell n(p/\bar{p}) \end{aligned} \tag{2.7}$$

In terms of these new variables, Eq. (2.5) may be rewritten in the form

$$R(\bar{\pi}) = \int_{-\infty}^{\infty} B(\pi)\ W(\bar{\pi}-\pi)\ d\pi \quad , \tag{2.8}$$

where

$$\begin{aligned} R(\bar{\pi}) &= R_i(\bar{p}) \quad , \\ B(\pi) &= B_i(p) \quad , \\ W(-\pi) &= W(p) \quad . \end{aligned} \tag{2.9}$$

We then perform a bilateral Laplace transformation on both sides of Eq. (2.8), viz.,

$$\begin{aligned} &\int_{-\infty}^{\infty} e^{-s\bar{\pi}}\ R(\bar{\pi})\ d\bar{\pi} \\ &\quad = \int_{-\infty}^{\infty} e^{-s\bar{\pi}} \left\{ \int_{-\infty}^{\infty} B(\pi)\ W(\bar{\pi}-\pi)\ d\pi \right\} d\bar{\pi} \quad . \end{aligned} \tag{2.10}$$

By virtue of the convolution theory for Laplace transform (Widder, 1971), we may deconvolute the right-hand side of Eq. (2.10) to obtain

$$r(s) = b(s)\ w(-s) \quad , \tag{2.11}$$

where

$$r(s) = \int_{-\infty}^{\infty} e^{-s\bar{\pi}}\ R(\bar{\pi})\ d\bar{\pi} \quad , \tag{2.12}$$

$$b(s) = \int_{-\infty}^{\infty} e^{-s\bar{\pi}}\ B(\bar{\pi})\ d\bar{\pi} \quad , \tag{2.13}$$

$$w(-s) = \int_{-\infty}^{\infty} e^{s\bar{\pi}} W(\bar{\pi})\, d\bar{\pi} \quad . \tag{2.14}$$

In deriving Eq. (2.11), there are a number of intricate sign changes so that the argument for w is $-s$ rather than s, and all the integrations are over the $\bar{\pi}$-space. The detailed derivations are in Appendix A. The quantities r(s), b(s), and w(-s) are the bilateral Laplace transforms of R, B, W, respectively. Since the integration of B and W in Eq. (2.10) has been deconvoluted, we may express b(s), which is related to the Planck intensity, in the form

$$b(s) = \frac{r(s)}{w(-s)} \quad , \tag{2.15}$$

so that

$$B(\bar{\pi}) = L^{-1}\left[\frac{r(s)}{w(-s)}\right] \quad , \tag{2.16}$$

where L^{-1} is the inverse bilateral Laplace transform. It is clear that once the functional forms for r(s) and w(-s), as well as the inverse formula for r(s)/w(-s) are known, the profile of $B(\pi)$ may be derived. One approach would be to expand the quantity 1/w(-s) into a MacLaurin series (Pearson, 1974), which is a form of Taylor's expansion with the reference point fixed at s = 0, in the form

$$\frac{1}{w(-s)} = \sum_{k=0}^{\infty} \lambda_k s^k \quad , \tag{2.17}$$

where the coefficient λ_k is related to the kth derivative of the function 1/w(-s) evaluated at s = 0, as follows:

$$\lambda_k = \left[\frac{1}{w(-s)} \right]^{(k)}_{s=0} / k! \quad . \tag{2.18}$$

Equation (2.17) may be substituted into Eq. (2.16) to obtain an expression for b(s) in terms of an infinite power series in the form

$$b(s) = \sum_{k=0}^{\infty} \lambda_k s^k r(s) \quad . \tag{2.19}$$

Thus, from Eq. (2.16), we have

$$B(\bar{\pi}) = \sum_{k=0}^{\infty} \lambda_k L^{-1} [s^k r(s)] \quad . \tag{2.20}$$

The Laplace transform of the kth derivative of a function R(x) can be expressed by (Abramowitz and Stegun, 1968)

$$L \left[\frac{d^k R(x)}{ds^k} \right] = s^k r(s) - \sum_{n=0}^{k-1} s^n R^{(k-1-n)}(x \to -\infty) \quad . \tag{2.21}$$

When $\bar{\pi} \to -\infty$, i.e., $\bar{p} \to \infty$, the upwelling radiance $R(\bar{\pi})$ does not exist in physical space. Thus, from Eq. (2.21), we have

$$L^{-1}[s^k r(s)] = R^{(k)}(\bar{\pi}) \quad . \tag{2.22}$$

The Planck intensity at a given level $\bar{\pi}$ is now expressible in terms of the linear sum of radiance derivatives at that level in the form

$$B(\bar{\pi}) = \sum_{k=0}^{\infty} \lambda_k R^{(k)}(\bar{\pi}) \quad . \tag{2.23}$$

The solution of $B(\bar{\pi})$ will be mathematically exact for infinite summations. It requires no constraint and is self-limited to the highest order of recoverable derivatives. In practice, since there are only a limited number of radiance measurements available for distinct values of $\bar{\pi}$, two error components may be entered into the retrieval. One is the instrument noise, while the other is the so-called "null-space" error, which is generated by an inadequate representation of $R^{(k)}(\bar{\pi})$ in the data-void $\bar{\pi}$-space. Both of these errors may be amplified or suppressed by the coefficients λ_k, depending on their magnitude.

2.3. Weighting Function and Inverse Coefficient

The determination of $B(\bar{\pi})$ from Eq. (2.23), requires knowledge of both the inverse coefficient λ_k and the derivatives of radiance $R^{(k)}(\bar{\pi})$. In this section, we shall focus on the discussion of the derivation of expressions for λ_k. We shall rewrite Eq. (2.14) in the form

$$w(-s) = \int_0^\infty \tilde{p}^{-s}\, W(\tilde{p})\, d\tilde{p}/\tilde{p} \quad , \tag{2.24}$$

where the spectral weighting function $W(\tilde{p})$ is defined by

$$W(\tilde{p}) = \int_{\Delta\nu_i} \left[\frac{\partial T_\nu(\tilde{p})}{\partial \ell n \tilde{p}}\right] \phi_i(\nu)\, d\nu \quad . \tag{2.25}$$

Note that in Eq. (2.24), the integration is over the $\tilde{p}$-space rather than the $\bar{\pi}$-space. Since $w(-s)$ is a function of s only, use of either $\tilde{p}$ or $\bar{\pi}$ is mathematically correct. In physical space, however, it is more appropriate to express W in terms of $\tilde{p}$. In principle, if the weighting

functions $W(\tilde{p})$ are known, e.g., through accurate line-by-line spectral integration, it is possible to evaluate $1/w(-s)$ and its derivatives numerically. Subsequently, λ_k can be computed from Eq. (2.18). In this manner, the potential error in λ_k would be minimal. However, for the purpose of analysis, it is desirable to develop an analytic form that can approximate the weighting functions associated with sounding channels without incurring significant errors. A generalized weighting function was proposed by King (1985) in the form

$$W(\tilde{p}) = m^{m-1} \Gamma^{-1}(m) \; \tilde{p} \exp [-m \tilde{p}^{1/m}] \quad , \tag{2.26}$$

where Γ is the Gamma function and m is an index controlling the sharpness of the weighting function. When m = 1 and 0.5, the weighting functions follow Goody-statistical and Elsasser-regular band models, respectively. The factor $m^{m-1} \Gamma^{-1}(m)$ in Eq. (2.26) normalizes the weighting function to unity and insures that $W = W_{max} = W(\tilde{p} = 1)$.

Figure 1 depicts the shapes of the generalized weighting functions for m = 0.5, 1, and 2. Large m values correspond to broader weighting functions, but smaller peak values. The peak values for m = 0.5, 1, and 2 are 0.484, 0.368, and 0.271, respectively. As shown in Fig. 1, the prime contribution of the weighting function comes from $0.1 < (\bar{p}/p) < 10$, a range of two orders of magnitude.

Using the generalized weighting function, we can show from Eq. (2.24) that

$$w(-s) = \Gamma[m(1-s)] \; / \; [\Gamma(m) \, m^{-ms}] \quad . \tag{2.27}$$

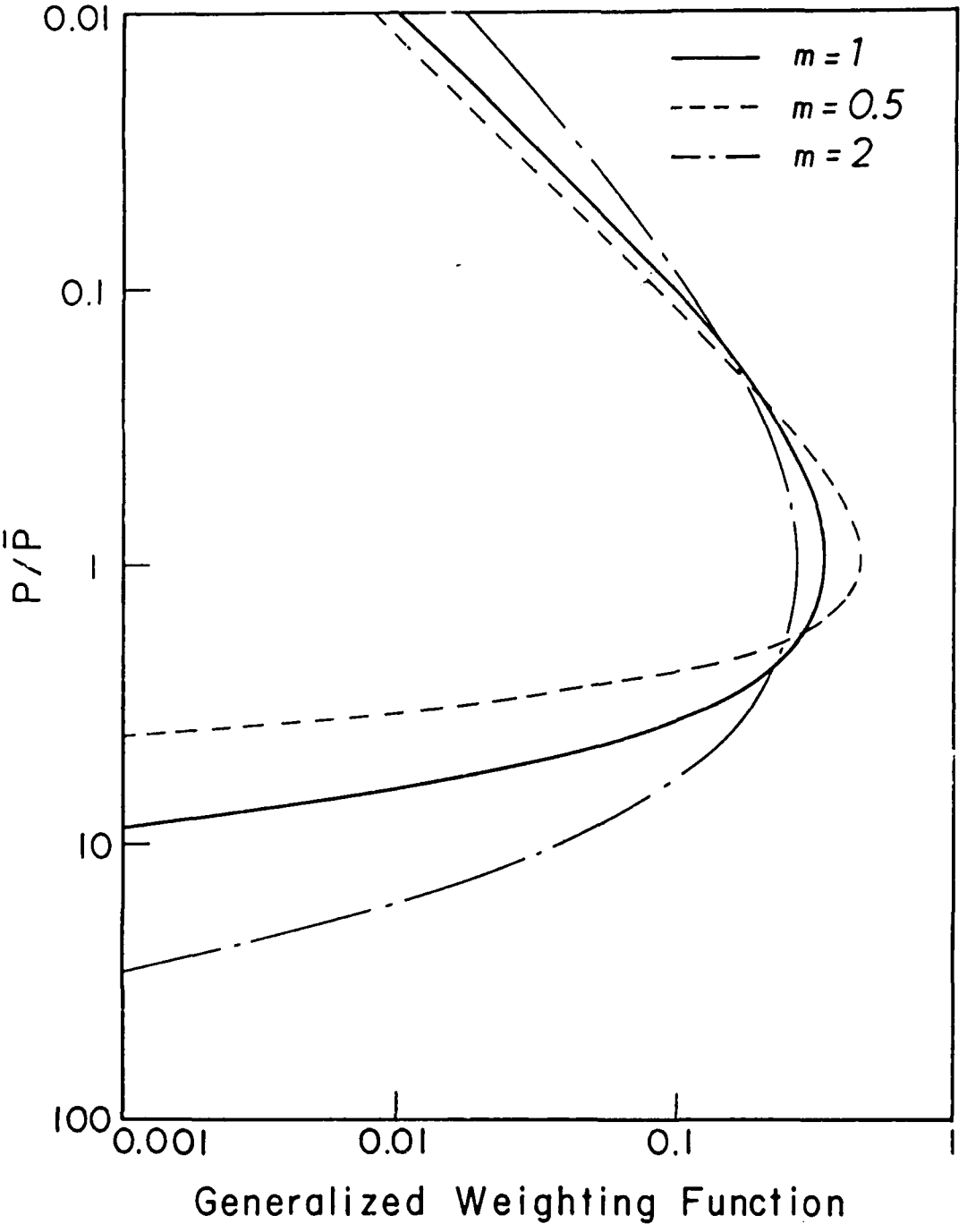

FIGURE 1. The generalized weighting function as a function of $p/\bar{p}$ for the parameter m of 0.5, 1, and 2.

The derivation of this form is given in Appendix B. Evaluation of the inversion coefficient λ_k, based on Eq. (2.27), requires derivatives of the Gamma functions, which are related to digamma and polygamma functions. The expressions for λ_k for k = 1 to 5 as functions of the index m have been derived and are given below:

$$\lambda_1 = m\,[\psi(m) - \ell n\ m] \quad , \tag{2.28}$$

$$\lambda_2 = \frac{\lambda_1^2}{2} - \frac{m^2}{2}\,\psi'(m) \quad , \tag{2.29}$$

$$\lambda_3 = \frac{\lambda_1^3}{6} - \frac{m^2\lambda_1}{2}\,\psi'(m) + \frac{m^3}{2}\,\psi''(m) \quad , \tag{2.30}$$

$$\lambda_4 = \frac{\lambda_1^4}{24} - \frac{m^2\lambda_1^2}{4}\,\psi'(m) + \frac{m^3\lambda_1}{6}\,\psi''(m) + \frac{m^4}{8}\,[\psi'(m)]^2 - \frac{m^4}{24}\,\psi'''(m) \quad , \tag{2.31}$$

$$\lambda_5 = \frac{\lambda_1^5}{120} - \frac{m^2\lambda_1^3}{12}\,\psi'(m) + \frac{m^3\lambda_1^2}{12}\,\psi''(m) + \frac{m^4}{8}\,\lambda_1\,[\psi'(m)]^2 - \frac{m^4}{24}\,\lambda_1\,\psi'''(m) - \frac{m^5}{12}\,\psi'(m)\,\psi''(m) + \frac{m^5}{120}\,\psi^{(4)}(m) \quad , \tag{2.32}$$

where $\psi(m)$, $\psi'(m)$, $\psi''(m)$, $\psi'''(m)$, and $\psi^{(4)}(m)$ are the digamma, trigamma, tetragamma, pentagamma, and hexagama functions, and are defined by

$$\psi^{(k)}(m) = \frac{d^k\psi(m)}{dm^k} = \frac{d^{k+1}}{dm^{k+1}}[\ell n\Gamma(m)]. \tag{2.33}$$

Tables for the values of $\psi^{(k)}(m)$ are available for $1 \leq m \leq 2$ and $k \leq 3$ (Abramowitz and Stegun, 1968). However for $m < 1$, $m > 2$, or $k > 3$, these polygamma functions must be evaluated using recurrence relationships and series expansions. We find

$$\psi^{(k)}(m) = \psi^{(k)}(m+1) + (-1)^{k+1}\, k!\, m^{-k-1}, \qquad m < 1, \tag{2.34}$$

$$\psi^{(k)}(m) = \psi^{(k)}(m-1) + (-1)^{k}\, k!\, (m-1)^{-k-1}, \qquad m > 1, \tag{2.35}$$

$$\psi^{(k)}(m+1) = (-1)^{k+1} \left[k!\, \zeta(k+1) - \frac{(k+1)!}{1!}\, \zeta(k+2)\, m + \frac{(k+2)!}{2!}\, \zeta(k+3)\, m^2 - \ldots \right], \quad k > 3 \tag{2.36}$$

where $\zeta(k)$ is the Riemann Zeta function, which is defined by

$$\zeta(k) = \sum_{n=1}^{\infty} n^{-k} \quad . \tag{2.37}$$

Figure 2 shows the inversion coefficients λ_k ($k = 1$-5) as functions of the index m. For any given m, λ_k may be obtained from this figure. For $0.1 < m < 1$, λ_k are within -1 and 0.2. Based on Eq. (2.23), any error incurred in $R^{(k)}(\pi)$ will be substantially reduced. This implies that for $0.1 < m < 1$, $B(\pi)$ will be relatively insensitive to errors in $R^{(k)}(\bar{\pi})$. For $m > 1$, $|\lambda_1|$, $|\lambda_3|$, and $|\lambda_5|$ are less than 1. However, $|\lambda_2|$ and $|\lambda_4|$ are larger than 1. Errors in $R^{(2)}(\bar{\pi})$ and $R^{(4)}(\bar{\pi})$ will then be greatly amplified through λ_2 and λ_4 and propagate into the computation of $B(\bar{\pi})$.

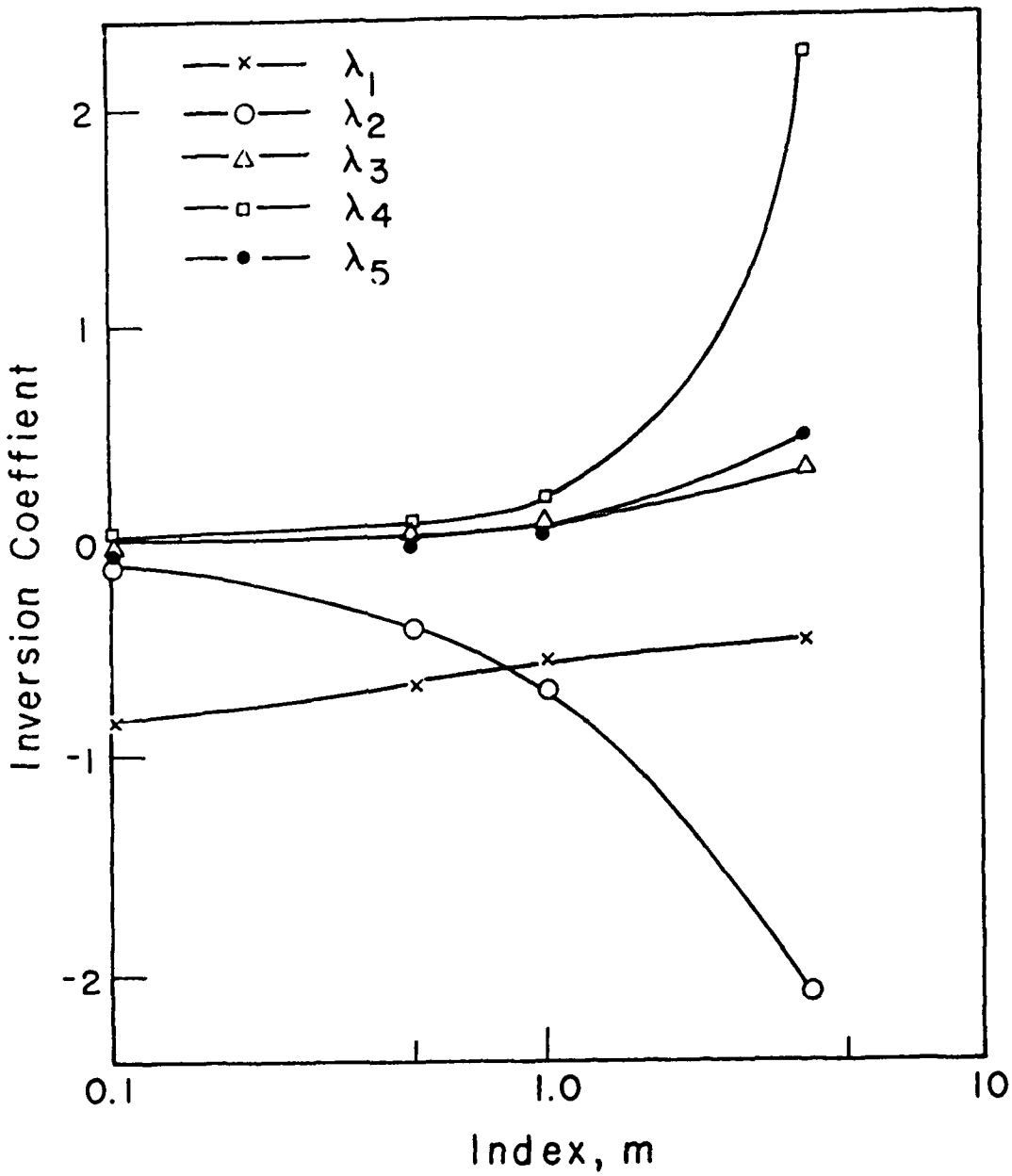

FIGURE 2. Inversion coefficients λ_i (i=1-5) as a function of the index m.

Section 3

APPLICATIONS OF THE DIM TO TEMPERATURE RETRIEVALS USING THE HIRS CHANNELS

In this section, we shall test the DIM by performing synthetic analyses using HIRS channels in the 15 μm CO_2 band. It is our objective to physically understand the generalization and determine the practicality of this method for temperature retrievals.

3.1 HIRS Channel Characteristics

In order to investigate the potential applicability of the DIM, HIRS channels (Smith et al., 1975) are used to perform the temperature retrieval. HIRS consists of seven channels in the 15 μm CO_2 band, and five channels in the 4.3 μm CO_2 band. We shall focus our investigation on the seven channels in the 15 μm CO_2 band. It is noted that the peaks of the weighting functions of these channels are more evenly distributed than those in the 4.3 μm band. The characteristics of these channels are listed in Table 1.

Table 1. HIRS channel characteristics.

Channel	ν (cm^{-1})	ν_1	ν_2	$\Delta\nu$	Principal Absorbers	Level of W_{max}
1	668	666	670	4	CO_2	30
2	679	674	684	10	CO_2	60
3	690	685	697	12	CO_2	100
4	702	696	712	16	CO_2	250
5	716	708	724	16	CO_2	500
6	732	724	740	16	CO_2/H_2O	750
7	748	740	756	16	CO_2/H_2O	900

3.2 Computation of Weighting Functions by the K-Correlated Method

In order to compute the transmittances and weighting functions, we used the absorption coefficient datasets computed by Chou and Kouvaris (1986) based on line-by-line data compiled by Rothman et al. (1983). The absorption coefficients due to CO_2 absorption are available for every 0.002 cm^{-1} between 540 and 800 cm^{-1} at 19 pressure levels (0.25-1000 mb for every $\Delta \log p = 0.2$) and three reference temperatures (210, 250, and 290 K). For each wavenumber and pressure level, the computed absorption coefficients were fitted to an empirical form of the temperature adjustment as follows:

$$k_\nu = \exp [a + b\Delta T + c\Delta T^2] \quad , \tag{3.1}$$

where $\Delta T = T-250$. The coefficients a, b, and c, obtained by curve fitting, are pressure and wavenumber dependent. Thus, the absorption coefficient for any wavenumber, pressure, or temperature can be obtained by interpolation between reference values.

Using the preceding absorption coefficients, the spectral transmittance and weighting function for a given pressure level p_i and for each HIRS channel may be computed by the following procedures. First, a table of k-distribution values for each of the 19 pressure levels and for each channel is compiled based on a reference atmospheric profile. The k-distribution is basically the probability of a certain k value in a small wavenumber interval. The determination of spectral transmittance over this interval does not depend on the position of each k value, but on its frequency of occurrence (Arking and Grossman, 1972).

Let f(k) be the probability density function, we may define a cumulative probability density function in the form

$$g(k) = \int_0^k f(k')\, dk' \quad . \tag{3.2}$$

It is noted that $g(0) = 0$ and $g(\infty) = 1$. In practice, for each channel and pressure level, we divide the logk-space into a large number of intervals of equal width. Using the k values calculated for every 0.002 cm^{-1}, we calculate, in a discrete manner, the k-distribution function for the ith Δlog k interval in the form

$$f(k_i)\ \Delta\log\ k_i = \frac{n(k_i)}{N} \quad , \tag{3.3}$$

where $n(k_i)$ is the number of wavenumber intervals ($\Delta\nu = 0.002\ cm^{-1}$) whose logk value falls between $\log k_i$ and $\log k_i + \Delta\log k_i$, and N is the total number of wavenumber intervals for a given channel. The cumulative g-function up to the ith interval can be obtained from

$$g(k_i) = \sum_{j=1}^{i} \frac{n(k_j)}{N} \quad , \ i > j. \tag{3.4}$$

The next step for calculating the transmittance or weighting function is based on the correlated k-distribution method (Lacis et al., 1979). For a homogeneous path, the spectrally averaged transmittance may be expressed by

$$T_{\bar{\nu}}(u) = \int_{\Delta\nu} e^{-k_\nu u}\ \frac{d\nu}{\Delta\nu} \quad . \tag{3.5}$$

As mentioned above, over a small spectral interval where the Planck intensity may be considered constant, the position of each k value has no bearing on the calculation of the spectral transmittance. Thus, the spectral integral may be transformed into the integral over the k-domain as follows:

$$T_{\bar{\nu}}(u) = \int_{k_{min}}^{k_{max}} e^{-ku} f(k)\, dk \quad , \tag{3.6}$$

where $f(k) = (dk/d\nu)^{-1}/\Delta\nu$. Based on the definition of the g-function denoted in Eq. (3.2), Eq. (3.6) may be rewritten in the form

$$T_{\bar{\nu}}(u) = \int_0^1 e^{-k(g)u}\, dg \quad . \tag{3.7}$$

If the relationship between k and g is known, the spectral transmittance $T_{\bar{\nu}}(u)$ can be evaluated.

However, for an inhomogeneous atmosphere, two assumptions must be made in order to obtain a form similar to Eq. (3.7). The spectral transmittance for an inhomogeneous atmosphere may be expressed by

$$T_{\bar{\nu}}(u) = \int_{\Delta\nu} \exp\left[-\int_0^u k_\nu(p,T)\, du' \right] \frac{d\nu}{\Delta\nu} \quad , \tag{3.8}$$

Let p_r and T_r denote the reference pressure and temperature, respectively. Then for any pair of (ν_i,ν_j), if $k_\nu(p_r,T_r)|\nu_i = k_\nu(p_r,T_r)|\nu_j$, it is assumed that $k_\nu(p,T)|\nu_i = k_\nu(p,T)|\nu_j$. This assumption implies that when the pressure and temperature change from the reference values (p_r,T_r)

to arbitrary values (p,T), the ratio $\tilde{k}(k_r,P,T) = k_\nu(p,T) \,/\, k_\nu(p_r,T_r)$ is a function of $k_\nu(p_r,T_r)(=k_r)$, p and T. Since k_r are known values, $\tilde{k}$ is independent of the wavenumber. Thus, the pathlength integral in the exponential argument in Eq. (3.8) may be scaled in the form

$$\int_0^u k_\nu(p,T)\, du' = k_r\, \tilde{u}\,(k_r,p,T) \quad , \tag{3.9}$$

where the scaled path length $\tilde{u}$ is defined by

$$\tilde{u}(k_r,p,T) = \int_0^u \tilde{k}\,(k_r,p,T)\, du' \quad . \tag{3.10}$$

In this way, the wavenumber dependence in k_r is separated from the pressure and temperature dependence in the pathlength integration. We may then transform the spectral integral in Eq. (3.8) into a k-space integral to obtain

$$T_{\bar{\nu}}(u) = \int_0^\infty \exp\,[-k(g_r)\,\tilde{u}]\, dg_r \quad , \tag{3.11}$$

where $g_r(k)$ is the accumulated probability density function for reference pressure and temperature. To perform numerical calculations using Eq. (3.11) further assumption must be made. For any pair of (ν_i, ν_j), if $k_\nu\,(p_r,T_r)|\nu_i > k_\nu(p_r,T_r)|\nu_j$, then $k_\nu(p,T)|\nu_i > k_\nu(p,T)|\nu_j$. This assumption, together with the previous one, allows us to express the following relationship:

$$\int_0^k f_r(k')\, dk' = \int_0^k f(k')\, dk' \quad , \tag{3.12}$$

or, from Eq. (3.2),

$$g_r(k) = g(k) \quad . \tag{3.13}$$

Based on the preceding assumptions, Eq. (3.11) may be rewritten in the form similar to Eq. (3.7) for homogeneous atmospheres:

$$\bar{T}_\nu(p) = \int_0^1 \exp\,[-k(g)\,\bar{u}]\, dg(k) \quad . \tag{3.14}$$

In practice, we use the g-function table for various pressure levels compiled in the first step, along with Eq. (3.13), to determine the correspondence between k and k_r. Then, for each g value, we determine the k_r value and a set of $\bar{k}(k_r,p,T)$ to compute the pathlength integration. Finally, the spectral transmittance is obtained by numerical integration according Eq. (3.14). This is referred to as the correlated k-distribution method. Lacis et al. (1979) showed that this method is remarkably accurate for the computation of transmittances and heating rates for the 9.6 μm ozone band.

In the present synthetic calculation, the transmittance for each HIRS channel is computed according to Eq. (3.14). The transmittance calculations using the correlated k-distribution are extremely efficient and accurate. The results are almost identical to those from line-by-line calculations (Liou et al., 1988). Figure 3 shows the weighting functions for seven HIRS channels, based on the U.S. standard atmospheric profile. The peak levels of these weighting functions are exactly the same as those listed in Table 1. It is noted that channel

1 peaks at the highest level and has the broadest weighting function, whereas channel 7 peaks near the surface and has the most narrow weighting function.

3.3 Computation of Inverse Coefficients Using the Generalized Weighting Function

It is possible to compute λ_k directly from Eqs. (2.14) and (2.18) using the weighting functions obtained from the correlated k-distribution method, but the computation could be very tedious. With the use of the generalized weighting function defined in Eq. (2.26), however, λ_k can be evaluated according to Eqs. (2.28)-(2.32) in a straightforward manner. We have developed a numerical method to fit HIRS weighting functions to the generalized form to obtain the index m associated with each channel. It is similar to the least-square method. We define the sum of the weighted square error at a given pressure level p_i in the form

$$E = \sum_{i=1}^{L} [W_m(\tilde{p}_i) - W(\tilde{p}_i)]^2 \epsilon_i \quad , \tag{3.15}$$

where L is the total number of pressure levels, $\tilde{p}_i = p_i/\bar{p}$, W_m and W are the generalized and computed weighting functions, respectively. The weight factor ϵ_i is prescribed as follows:

$$\epsilon_i = \begin{cases} \exp(-\tilde{p}_i) & , \tilde{p}_i > 1 \\ \exp(-\tilde{p}_i^{-1}) & , \tilde{p}_i < 1 \end{cases} \tag{3.16}$$

In this way, more weight is placed on the error near the weighting function peak ($\tilde{p}_i = 1$) than in the wing region. This is appropriate

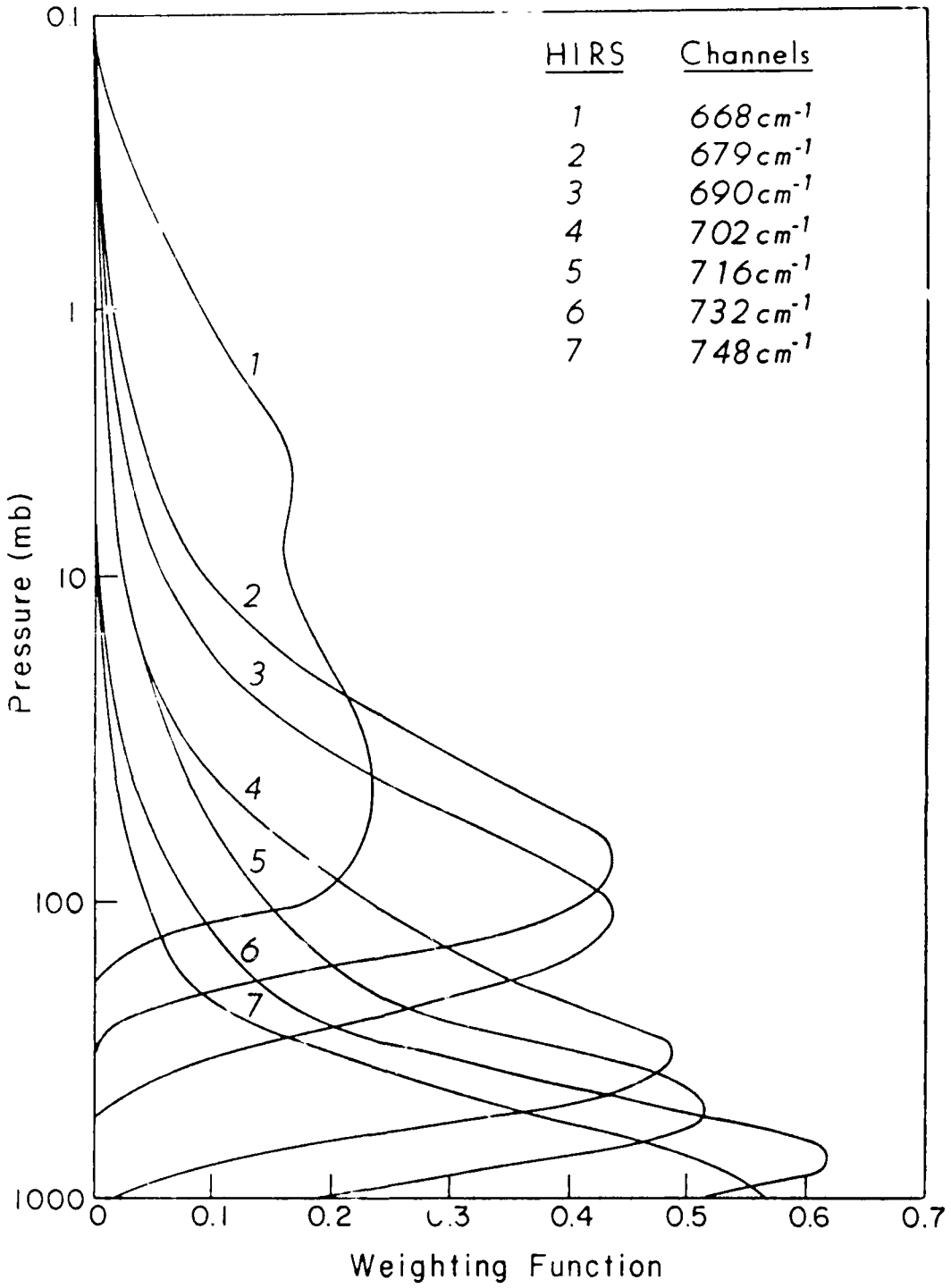

FIGURE 3. The weighting function of seven HIRS channels in the logarithmic pressure coordinate. The peaks of these weighting functions are listed in Table 1.

since, in computing the upwelling radiance, the greatest contribution comes from the weighting function peak level. We then proceed to minimize E, such that

$$\frac{\partial E}{\partial m} = 0 \ , \tag{3.17}$$

which leads to

$$\sum_{i=1}^{L} 2 \left[W_m(\tilde{p}_i) - W(\tilde{p}_i)\right] \epsilon_i \, W_m(\tilde{p}_i) \ .$$

$$\left(1 - 1/m - (\tilde{p}_i)^{1/m} \left[1 - \ell n \, (\tilde{p}_i)/m\right] + \ell nm - \psi(m)\right) = 0, \tag{3.18}$$

where $\psi(m)$ is the digamma function. The derivation of Eq. (3.18) is given in Appendix C.

Equation (3.18) is a complicated, nonlinear algebraic equation, and can only be solved by a numerical root-finding method. Although Newton's iteration method is the most efficient, it requires specification of the functional form of the second-order derivative of E, which in the present case is much more complicated than the first-order derivative. For any channel, m will be within 0.1 and 4 as shown in Table 2. Thus, we may use the bisection method described by Hamming (1973) to solve for m. The details of the bisection method used in the fitting are given in Appendix D. Table 2 lists the values of the parameter m for each HIRS channel, RMS error, peak value of $W(\tilde{p}_i)$, and error near the peak of the weighting function. The RMS error is defined by

Table 2. Values of parameter m, RMS error, and error near the peak weighting function for the HIRS channels.

Channel	m	RMS error	W_{max}*	error near peak
1	2.8370	0.0141	0.234	-0.0036
2	0.6410	0.0137	0.433	0.0073
3	0.6668	0.0107	0.436	0.0017
4	0.4570	0.0237	0.487	-0.0129
5	0.4273	0.0137	0.517	-0.0048
6	0.2305	0.0159	0.614	0.0076
7	0.3160	0.0118	0.566	-0.0004

*W_{max} denotes the maximum value of the weighting function.

$$e = \left\{ \frac{1}{L} \sum_{i=1}^{L} [W_m(\tilde{p}_i) - W(\tilde{p}_i)]^2 \right\}^{1/2} . \qquad (3.19)$$

The RMS errors for all channels are within about 0.01-0.02. Such errors are sufficiently small to have a significant effect on the upwelling radiance calculation. The effect of the weight factor ϵ_i is reflected by the fact that the error near the peak for each channel is smaller in magnitude than the corresponding RMS error. For channel 1, a large m is found, which corresponds to a broad weighting function. For other channels, m ranges from 0.2 to 0.7. It is apparent that neither the random model nor the regular model can fit the HIRS channel transmittance well. Based on the m values, the inversion coefficient λ_k may be evaluated for each channel (see Fig. 2). These λ_k values are tabulated in Table 3. Note that all $|\lambda_k|$ are less than 1, except $|\lambda_2|$ and $|\lambda_4|$ for channel 1. Thus, it is anticipated that the retrieved temperature at 30 mb, which is the peak level of weighting function for channel 1,

Table 3. Inversion coefficient values, λ_k, for the seven HIRS channels.

Channel	λ_1	λ_2	λ_3	λ_4	λ_5
1	-0.52	-1.60	0.21	1.44	0.270
2	-0.60	-0.48	0.01	0.06	0.017
3	-0.61	-0.50	0.01	0.07	0.018
4	-0.63	-0.39	0.00	0.04	0.009
5	-0.63	-0.37	0.00	0.04	0.007
6	-0.70	-0.27	-0.01	0.03	0.001
7	-0.67	-0.32	-0.01	0.03	0.003

will be very sensitive to the measurement noise and errors in the radiance fitting.

3.4 Synthetic Computation of Channel Radiances

To test the reliability and applicability of the DIM, real-time satellite radiance data must be used. At the same time, the retrieved temperature profiles must be verified with the ground-truth. Before the application of real data, we shall use a set of radiance values obtained from synthetic computations to explore the feasibility of the DIM for temperature retrievals. Let R_i be the radiance associated with the ith sounding channel whose value may be computed from Eq. (2.5). The U.S. Standard Atmospheric Temperature is used as the reference profile. Table 4 lists the computed upwelling radiances for the seven These radiances increase from the band center to the wing.

Table 4. Radiance values for HIRS channels.

Channel	Radiance $R_i \Delta\nu_i$ (erg/cm^2-sec-sr)
1	224
2	437
3	513
4	818
5	999
6	1230
7	1420

3.5 Polynomial Fitting of Radiances

It is necessary to develop a curve-fitting method to fit the seven upwelling radiances, since higher-order derivatives are required to calculate the Planck intensity. Several numerical methods are available for the present purpose, and can be divided into two categories. The first is the spline method, which fits selected radiance values in a piece-wise manner. The curve segments between successive radiance values are smooth without oscillations incurred by higher-order polynomial fittings. If the cubic spline method is used, an assumption about the derivatives at the endpoint must be made. We may obtain at most third-order derivatives, since all higher-order derivatives vanish. The second category is associated with the polynomial fitting. This method fits all radiance values to a single polynomial.

In the present study, we use the Newtonian interpolation scheme (Hamming, 1973) in view of its simplicity in the determination of higher-order derivatives. The Newtonian interpolation scheme uses a polynomial in the form

$$R = R_1 + \sum_{k=1}^{K} R_1^{(k)} \prod_{j=1}^{k} (\bar{\pi} - \bar{\pi}_j) \quad , \tag{3.20}$$

where R_1 is the radiance for channel 1, K the order of the polynomial, $R_1^{(k)}$ the pseudo-derivative of order k, $\bar{\pi} = -\ell n\bar{p}$, and $\bar{\pi}_j = -\ell n\bar{p}_j$. The pseudo-derivatives $R_1^{(k)}$ are defined by

$$R_1^{(1)} = \frac{R_2 - R_1}{\pi_2 - \pi_1} \; ; \quad R_i^{(1)} = \frac{R_{i+1} - R_i}{\pi_{i+1} - \pi_i} \quad , \quad 1 < i < K-1$$

$$R_1^{(2)} = \frac{R_2^{(1)} - R_1^{(1)}}{\pi_3 - \pi_1} \; ; \quad R_i^{(2)} = \frac{R_{i+1}^{(1)} - R_i^{(1)}}{\pi_{i+1} - \pi_i} \quad , \; 1 < i < K-2$$

$$\vdots$$

$$R_1^{(K-1)} = \frac{R_2^{(K-2)} - R_1^{(K-2)}}{\pi_K - \pi_1} \quad , \tag{3.21}$$

where R_i is the radiance for the ith channel. On the basis of the preceding definition, if K = 1, the polynomial will give the exact radiance values for the first two channels. If K = 6, the exact radiance values for all seven channels will be produced.

Figure 4 shows the curves of the fitted first-, third-, and fifth-order polynomials based on the seven radiance values listed in Table 4. It is evident that the fifth-order polynomial fits the radiance values best. However, fluctuations occur between channels 1 and 3. This suggests that a smooth curve-fitting method could be advantageous in the inversion exercises because higher-order derivatives of the curve are needed in order to compute the Planck intensity. Based on Eq.

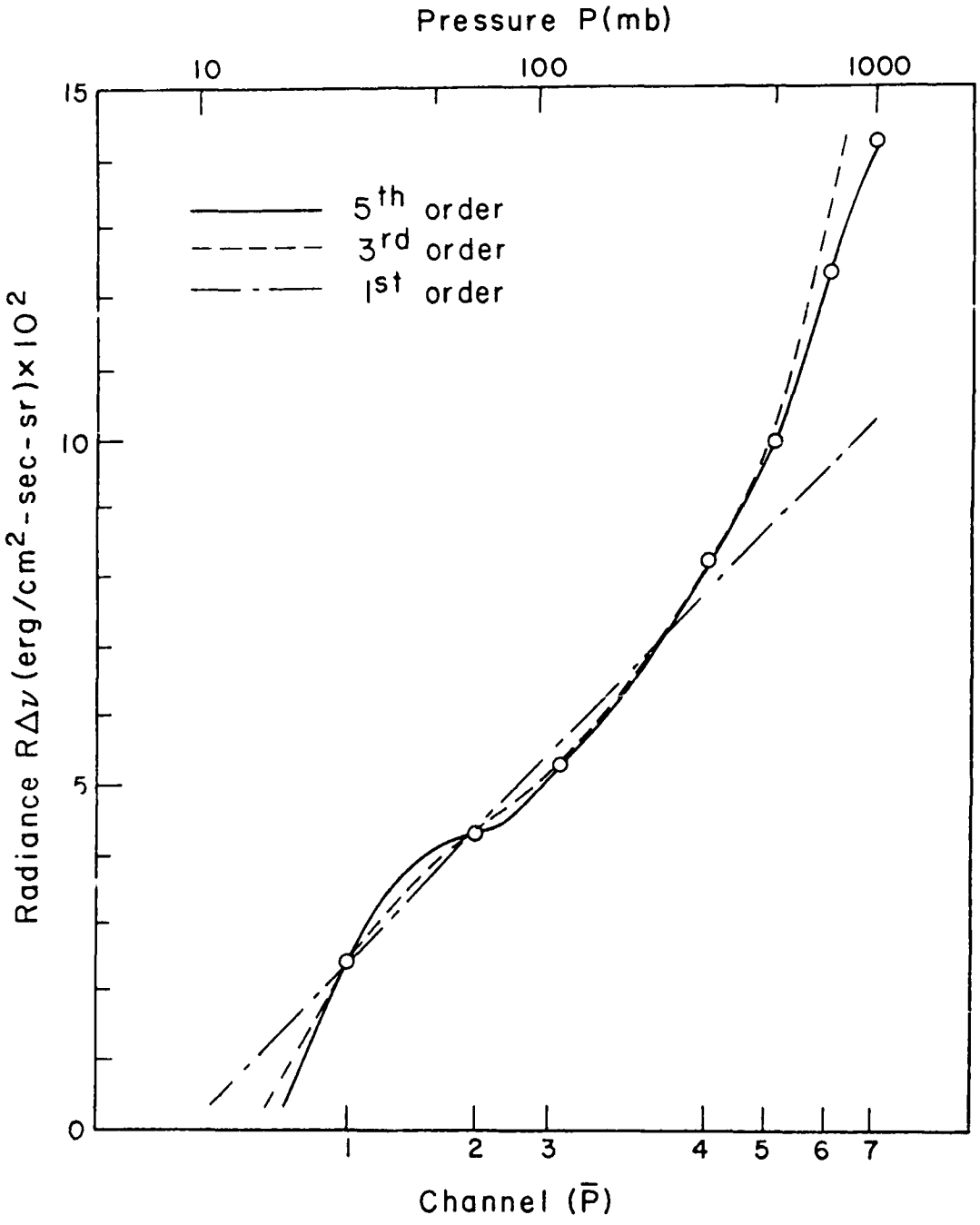

FIGURE 4. The computed upwelling radiances (circles) for seven HIRS channels in the logarithmic pressure coordinate, and curve fittings to the computed values using first-, third-, and fifth-order polynomials. The U.S. standard temperature is used in the computation.

(3.20), analytic expressions for the higher-order derivatives may be derived and are given in Appendix E.

3.6 Inversion Exercise Using the Generalized Weighting Function

Since the inversion coefficients λ_k are known, as are the derivatives, the Planck intensity $B(\bar{\pi}_i)$ at the peak of the weighting function for each channel can be computed from Eq. (2.23). From the Planck intensity, the temperature can be evaluated from

$$T(\bar{\pi}_i) = hc\,\bar{\nu}_i \,/\, \{K\,\ell n\,[1 + 2hc^2\,\bar{\nu}_i^3 \,/\, B(\bar{\pi}_i)]\} \quad , \tag{3.22}$$

where the quantities h, c, $\bar{\nu}_i$, and K represent the Planck constant, speed of light in vacuum, central wavenumber of the ith channel, and Boltzmann constant, respectively.

Figure 5 shows retrieval results for the first-, third-, and fifth-order polynomial fittings to synthetic HIRS radiances using the U.S. standard atmospheric profile. It is quite encouraging to find that the retrieval results converge to the true temperature in the lower troposphere as higher-order radiance derivatives are incorporated in the calculation. For the fifth-order approximation, errors in the retrieved temperatures in the lower troposphere, corresponding to channels 4 to 7, are within about 2 K. Retrieved temperatures associated with channels 1-3 show larger deviations from the true temperature values. The large deviations in the upper atmosphere are primarily caused by the "null-space" error of the higher-order derivatives, associated with the less satisfactory polynomial fitting between radiances for channels 1 and 3, as noted in Fig. 4.

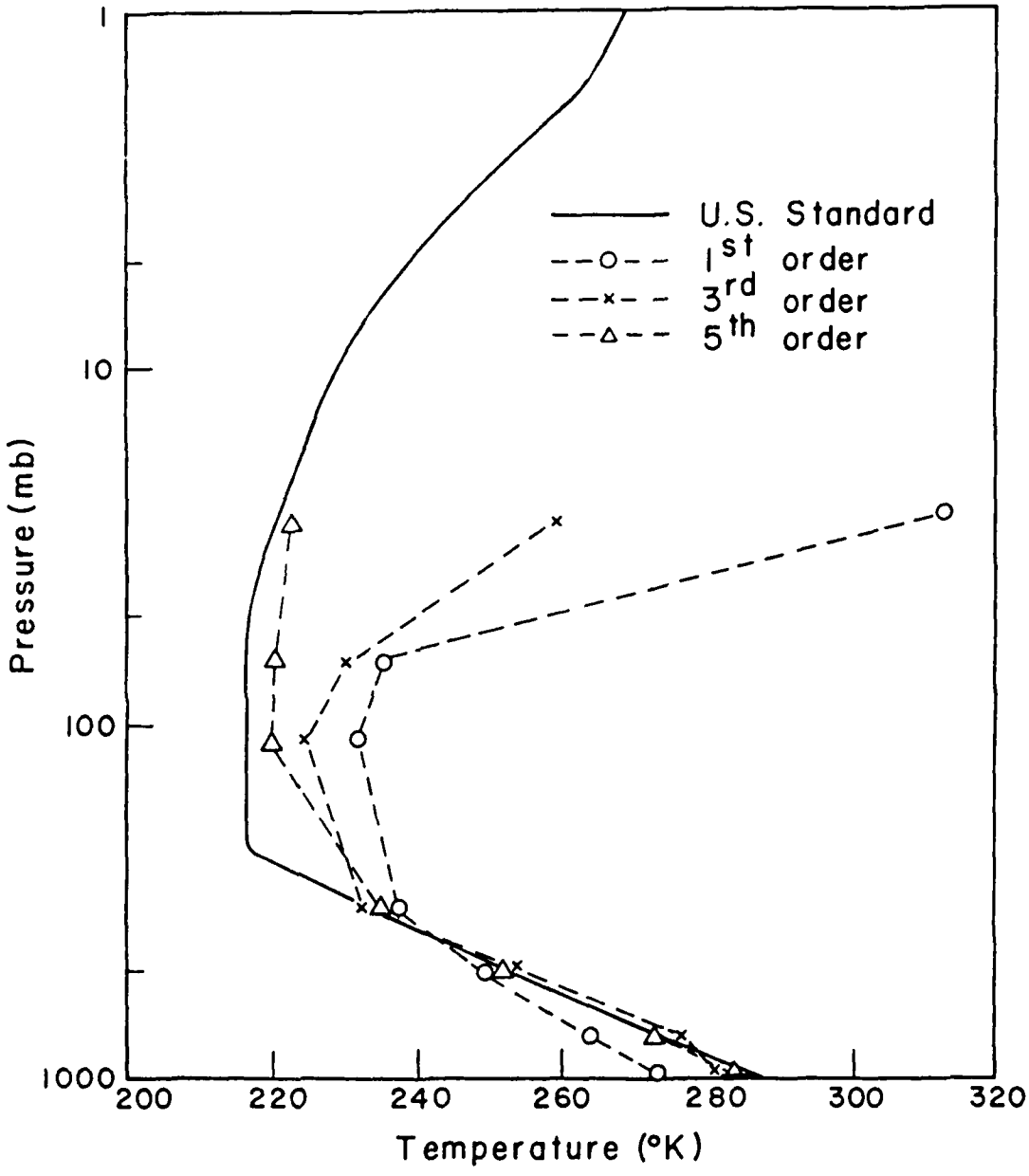

FIGURE 5. Results of DIM temperature retrievals using first-, third-, and fifth-order expansions for the U.S. standard temperature profile.

To further test the practical applicability of the DIM, we performed a similar retrieval exercise using the tropical atmospheric profile (McClatchey et al., 1971). As shown in Fig. 6, the tropical temperature profile differs significantly from the standard atmospheric profile. Most notable is the strong inversion of the tropopause near the 100 mb level. Again, the retrieved solution converges to the true profile in the lower troposphere when the higher-order derivatives are added to the series expansion. The retrieved temperatures are within about 1 K for channels 4-7. However, errors in the temperature at the top three levels are even larger than those in the standard atmosphere. This is because the effect of the strong temperature inversion at the tropopause cannot be properly accounted for in the polynomial fitting.

Based on the two cases presented above, errors in the generalized weighting functions for channels 4-7 have negligible effects on the retrieved temperature profile. However, a better polynomial representation is required to improve the retrieval of temperatures at the top three levels.

3.7 Effects of Random Errors

Finally, we perform retrieval analyses by adding random errors to the radiance values. Maximum random errors of 2 and 5% were used. The resulting temperature errors are shown in Fig. 7. Except for channel 1, the addition of random errors does not produce significant errors in temperature retrievals. This is particularly evident for channels 4-7, where peaks of the weighting function are in the lower atmosphere. The inability to perform retrievals for channel 1 when random errors are added is due to the nature of the broad weighting function. In this

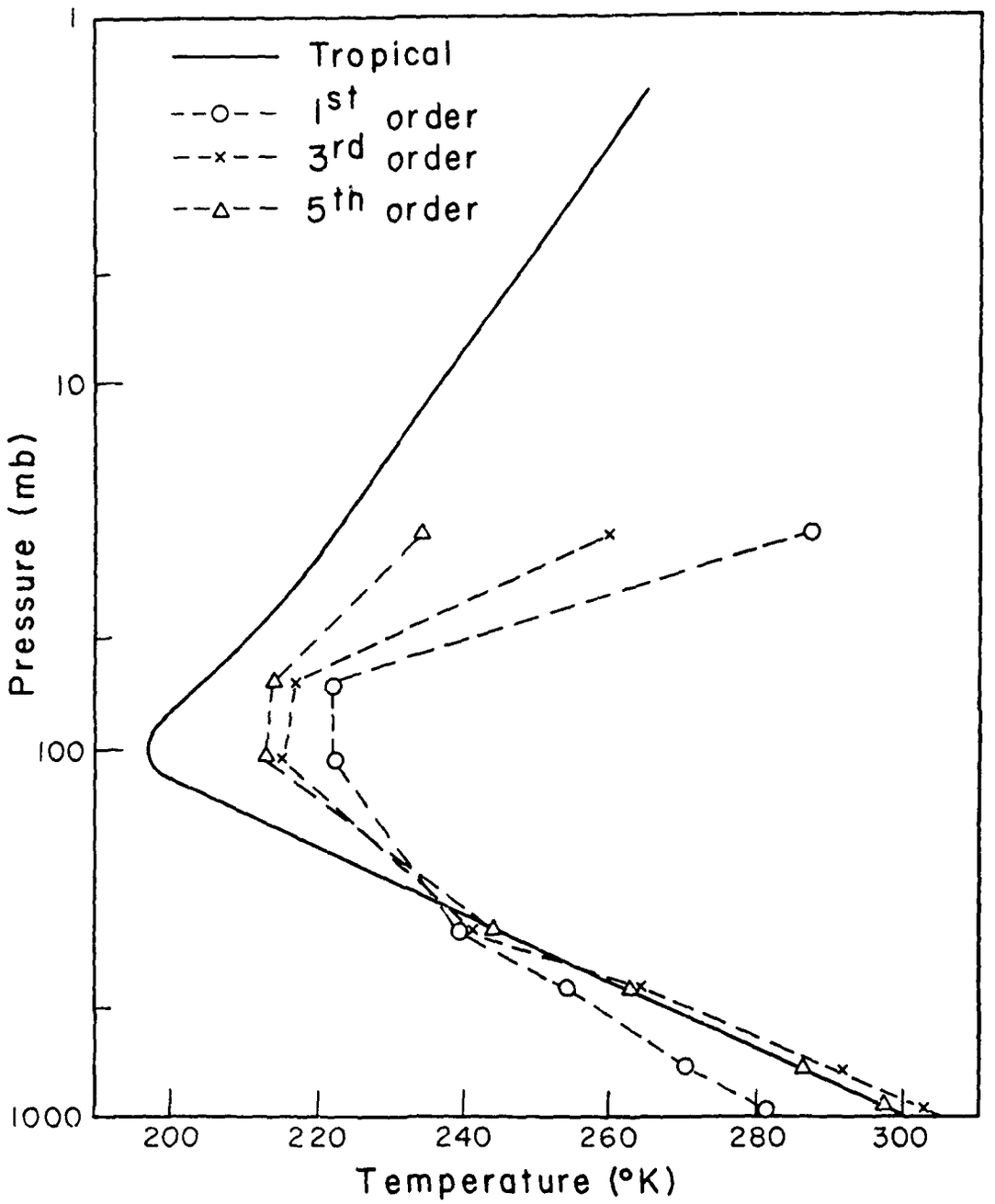

FIGURE 6. Same as Fig. 5, except for the tropical temperature profile.

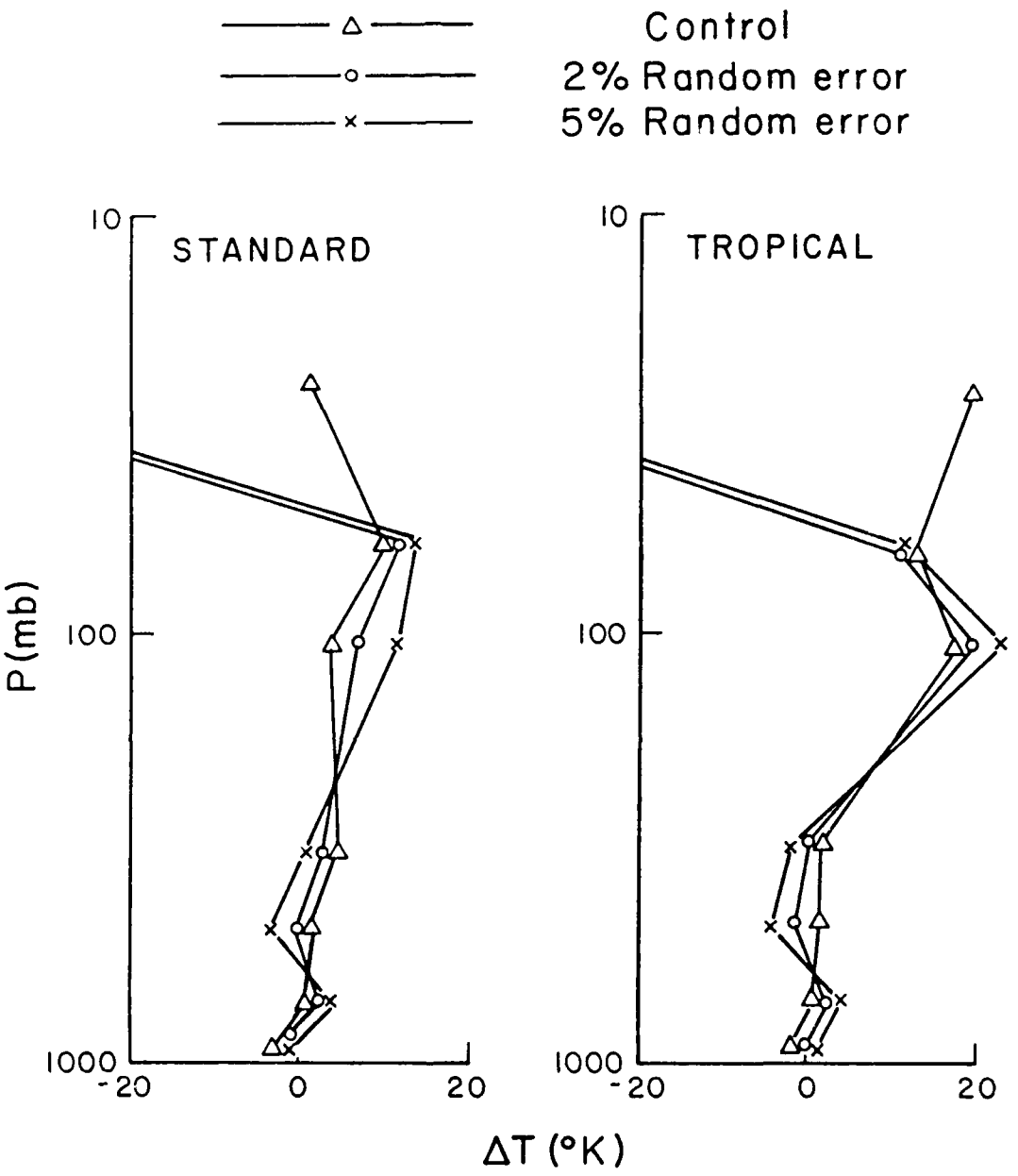

FIGURE 7. Analyses of errors for DIM temperature retrievals with and without random errors. Maximum random errors of 2 and 5% are used in the calculation.

case, the parameter $m \doteq 2.8$, and λ_k have large negative and positive values, as shown in Fig. 2. As a result, small errors in radiance values are amplified and propagate onto the retrieved Planck intensity, leading to unstable results for this channel.

Section 4

CONCLUSION

In this report we have presented the differential inversion method (DIM) for temperature retrievals in terms of the theory of radiative transfer. It is shown that, in the Laplace transform space, the Planck intensity is directly related to the upwelling radiance weighted by the weighting function. After expanding the transformed weighting function in a MacLaurin series and performing the inverse transform, the Planck intensity in real space can be exactly expressed by a linear combination of the derivatives of radiances.

Using seven HIRS channels in the 15 μm CO_2 band, we have performed numerical analyses for temperature retrievals, including the curve-fitting of seven radiance values. We demonstrate that a fifth-order polynomial fitting to radiance values is adequate to yield correct retrieval results for temperature and that the DIM converges to the true temperature solution. In retrieval exercises, two distinct temperature profiles (U.S. Standard and Tropical) were used. The retrieved temperatures in the troposphere, corresponding to channels 4-7 are accurate within 1-2 K. Addition of random errors with a maximum value of 5% to the radiance values does not introduce instability in the inversion exercises. One exception is channel 1, corresponding to the center of the 15 μ CO_2 band, which has a broad weighting function. This appears to suggest that the DIM is particularly useful and practical for sharp weighting functions. Our preliminary conclusion is

Appendix A

DERIVATION OF EQ. (2.11)

We rewrite Eq. (2.10) in the form

$$r(s) = \int_{-\infty}^{\infty} e^{-s\bar{\pi}} \left\{ \int_{-\infty}^{\infty} B(\pi)\, W(\pi-\bar{\pi})\, d\pi \right\} d\bar{\pi} \quad , \tag{A.1}$$

where

$$r(s) = \int_{-\infty}^{\infty} e^{-s\bar{\pi}}\, R(\bar{\pi})\, d\bar{\pi} \quad .$$

The right-hand side of Eq. (A.1) is the bilateral Laplace transform of a convoluted integral function. Since

$$e^{-s\bar{\pi}} = e^{-s\pi} \cdot e^{s(\pi-\bar{\pi})} \quad , \tag{A.2}$$

We may rewrite Eq. (A.1) as follows:

$$r(s) = \int_{-\infty}^{\infty} e^{-s\pi}\, B(\pi) \left\{ \int_{-\infty}^{\infty} e^{s(\pi-\bar{\pi})}\, W(\pi-\bar{\pi})\, d\pi \right\} d\pi \quad . \tag{A.3}$$

The term in the braces is the bilateral Laplace transform of W and may be expressed by

$$\int_{-\infty}^{\infty} e^{s(\pi-\bar{\pi})}\, W(\pi-\bar{\pi})\, d\bar{\pi} = \int_{-\infty}^{\infty} e^{sy}\, W(y)\, dy = w(-s) \quad , \tag{A.4}$$

where $y = \pi - \bar{\pi}$, $dy = -d\bar{\pi}$, $y \to -\infty$ as $\bar{\pi} \to \infty$, and $y \to \infty$ as $\bar{\pi} \to -\infty$. Substituting Eq. (A.4) into Eq. (A.3), we obtain

$$r(s) = b(s)\, w(-s) \quad , \tag{A.5}$$

where

$$b(s) = \int_{-\infty}^{\infty} e^{-s\bar{\pi}}\, B(\bar{\pi})\, d\bar{\pi} \quad , \tag{A.6}$$

$$w(-s) = \int_{-\infty}^{\infty} e^{s\bar{\pi}}\, W(\bar{\pi})\, d\bar{\pi} \quad . \tag{A.7}$$

Note that the integrations of Eqs. (A.6) and (A.7) are over the $\bar{\pi}$-space. This is because the integral in the braces of Eq. (A.1) is a function of $\bar{\pi}$ instead of π. Thus, b(s) and w(-s) are transformed from the $\bar{\pi}$-space to the s-space, and the inverse Laplace transform of b(s) should be $B(\bar{\pi})$ rather than $B(\pi)$.

Appendix B

DERIVATION OF THE LAPLACE TRANSFORM OF THE GENERALIZED WEIGHTING FUNCTION

On substituting Eq. (2.26) into Eq. (2.24), we obtain

$$w(-s) = m^{m-1}\,\Gamma^{-1}(m)\int_0^{\infty} \tilde{p}^{-s+1-1}\exp\left[-m\,\tilde{p}^{1/m}\right]\,d\tilde{p} \quad . \tag{B.1}$$

In order to fit the integration in Eq. (B.1) to a form of the Gamma function, we introduce the variable $x = m\,\tilde{p}^{1/m}$, so that $\tilde{p} = (x/m)^m$, and $d\tilde{p} = m^{-m+1}\,x^{m-1}\,dx$. Equation (B.1) then becomes

$$w(-s) = \Gamma^{-1}(m)\int_0^{\infty} x^{-ms}\,m^{ms}\,e^{-x}\,x^{m-1}\,d^x \quad , \tag{B.2}$$

Since

$$\int_0^{\infty} x^{-ms+m-1}\,e^{-x}\,d^x = \Gamma[m(1-s)] \quad , \tag{B.3}$$

we have from Eq. (B.2),

$$w(-s) = \Gamma^{-1}(m)\,\Gamma[m(1-s)]\,m^{ms} \quad . \tag{B.4}$$

Appendix C

DERIVATION OF EQ. (3.18)

From Eq. (3.15) the derivative $\partial E/\partial m$ is given by

$$\frac{\partial E}{\partial m} = \sum_{i=1}^{L} 2[W_m(\tilde{p}_i) - W(\tilde{p}_i)]\, \epsilon_i \frac{\partial W_m(\tilde{p}_i)}{\partial m} \quad . \tag{C.1}$$

We then rewrite Eq. (2.26) in the form

$$W_m(\tilde{p}_i) = \tilde{p}_i\, X(m)\, Y(m)\, Z(m) \quad , \tag{C.2}$$

where

$$X(m) = m^{m-1} \quad , \tag{C.3}$$

$$Y(m) = \Gamma^{-1}(m) \quad , \tag{C.4}$$

$$Z(m) = \exp\left(-m\, \tilde{p}_i^{\,1/m}\right) \quad . \tag{C.5}$$

Differentiation of Eq. (C.2) leads to

$$\frac{\partial W_m(\tilde{p}_i)}{\partial m} = \tilde{p}_i\, (X'YZ + XY'Z + XYZ') \quad , \tag{C.6}$$

where

$$X' = X\, (\ell n\, m + 1 - 1/m) \quad , \tag{C.7}$$

$$Y' = Y\, \psi(m) \quad , \tag{C.8}$$

$$Z' = Z\, \tilde{p}^{1/m}\, (1/m\, \ell n\, \tilde{p}_i - 1) \quad , \tag{C.9}$$

On substituting Eqs. (C.7)-(C.9) into Eq. (C.6), we obtain

$$\frac{\partial W_m(\tilde{p}_i)}{\partial m} = W_m(\tilde{p}_i) \left[\ell n\ m + 1 - 1/m - \psi(m) + \tilde{p}_i^{1/m} (1/m\ \ell n\ \tilde{p}_i - 1) \right] \quad . \tag{C.10}$$

Further substitution of Eq. (C.10) into Eq. (C.1) yields

$$\frac{\partial E}{\partial m} = \sum_{i=1}^{L} 2[W_m(\tilde{p}_i) - W(\tilde{p}_i)]\ \epsilon_i\ W_m \ ,$$

$$\left[\ell n\ m+1 - 1/m - \psi(m) + \tilde{p}_i^{1/m} (1/m\ \ell n\ \tilde{p}_i - 1) \right] \quad . \tag{C.11}$$

Appendix D

NUMERICAL SOLUTION OF EQ. (3.18)

The bisection method is used to solve Eq. (3.18) for the reason given in the main text. Let the derivative $\partial E/\partial m$ be designed as $f(m)$. We start from an initial guess $m^{[0]} = 0.1$, and obtain the function value $f^{[0]} = f(m^{[0]})$. Examination of the function $\partial E/\partial m$, reveals that $\partial E/\partial m > 0$ for small m, because $W_m(\tilde{p}_i) > W(\tilde{p}_i)$ near the peak and the dominant term $-\tilde{p}_i^{1/m}[1 - (\ell n\, \tilde{p}_i)/m] > 0$. Thus, if $f^{[0]} > 0$, $m^{[0]}$ will be too small. We then try another value, $m^{[1]}$, such that $m^{[1]} > m^{[0]}$, and obtain $f^{[1]}$. If $f^{[1]} > 0$, the process continues until, for a certain $m^{[n]}$, $f^{[n]} < 0$, but $f^{[n-1]} > 0$. From the mean value theorem, the solution for m must lie between $m^{[n-1]}$ and $m^{[n]}$. Subsequently, we try $m^{[n+1]} = 0.5\,(m^{[n-1]} + m^{[n]})$. If $f^{[n+1]} < 0$, we try $m^{[n+2]} = 0.5\,(m^{[n+1]} + m^{[n-1]})$. The process then continues until $f^{[m]} < \gamma$, where γ is a prescribed convergence criterion and M the total number of iterations. The value $m^{[M]}$ is then the solution for m.

Appendix E

EXPRESSIONS FOR THE HIGH-ORDER DERIVATIVES OF RADIANCES

The following expressions for the higher-order derivatives of radiances are derived from Eq. (3.20). Equations (E.1) and (E.2) are for the first- and second-order derivatives, respectively. Equation (E.3) is for the hth order derivative.

$$R' = R_1' + \sum_{i=1}^{2} (\bar{\pi}-\bar{\pi}_i)\, R_1''$$

$$+ \sum_{i=1}^{2} \sum_{\substack{j=2 \\ j>i}}^{3} (\bar{\pi}-\bar{\pi}_i)\,(\bar{\pi}-\bar{\pi}_j)\, R_1'''$$

$$+ \cdots$$

$$+ \sum_{i=1}^{2} \sum_{\substack{j=2 \\ j>i}}^{3} \cdots \sum_{\ell=k-2}^{K-1} \sum_{\substack{k=k-1 \\ k>\ell}}^{K} (\bar{\pi}-\bar{\pi}_i)\,(\bar{\pi}-\bar{\pi}_j) \cdots (\bar{\pi}-\bar{\pi}_\ell)\,(\bar{\pi}-\bar{\pi}_k)\, R_1^{(k)} \qquad \text{(E.1)}$$

$$R'' = 2R_1'' + 2 \sum_{i=1}^{3} (\bar{\pi}-\bar{\pi}_i)\, R_1'''$$

$$+ 2 \sum_{i=1}^{3} \sum_{\substack{j=2 \\ j>i}}^{4} (\bar{\pi}-\bar{\pi}_i)\,(\bar{\pi}-\bar{\pi}_j)\, R_1^{(4)}$$

$$+ \cdots$$

$$+ 2 \sum_{i=1}^{3} \sum_{\substack{j=2 \\ j>i}}^{4} \cdots \sum_{\ell=k-3}^{K-1} \sum_{\substack{k=k-2 \\ k>\ell}}^{K} (\bar{\pi}-\bar{\pi}_i)\,(\bar{\pi}-\bar{\pi}_j) \cdots (\bar{\pi}-\bar{\pi}_\ell)\,(\bar{\pi}-\bar{\pi}_k)\, R_1^{(k)} \qquad \text{(E.2)}$$

$$+ \cdots$$

$$R^{(h)} = h!\ \{R_1^{(h)} + \sum_{i=1}^{h+1} (\bar{\pi}-\bar{\pi}_i)\ R_1^{(h+1)}\}$$

$$+ \sum_{i=1}^{h+1} \sum_{\substack{j=2 \\ j>1}}^{h+2} (\bar{\pi}-\bar{\pi}_i)\ (\bar{\pi}-\bar{\pi}_j)\ R_1^{(h+2)}$$

$$+ \cdots$$

$$+ \sum_{i-1}^{h+1} \sum_{\substack{j=2 \\ j>i}}^{h+2} \cdots \sum_{\ell=k-h-1}^{K-1} \sum_{\substack{k=k-h \\ k>\ell}}^{K} (\bar{\pi}-\bar{\pi}_i)\ (\bar{\pi}-\bar{\pi}_j) \cdots (\bar{\pi}-\bar{\pi}_\ell)\ (\bar{\pi}-\bar{\pi}_k)\ R_1^{(k)}\} \qquad \text{(E.3)}$$

REFERENCES

Abramowitz, M. and I.E. Stegun, 1968: Handbook of Mathematical Functions. Dover, New York, 1045 pp.

Arking, A. and K. Grossman, 1971: The influence of the line change and band structure on temperatures in planetary atmospheres. J. Atmos. Sci., 29, 937-949.

Chahine, M., 1970: Inverse problems in radiative transfer: Determination of atmospheric parameters. J. Atmos. Sci., 27, 960-967.

Chou, M.D. and L. Kouvaris, 1986: Monochromatic calculations of atmospheric radiative transfer due to molecular line absorption. J. Geophys. Res., 91, 4047-4055.

Conrath, B.J., 1972: Vertical resolution of temperature profiles obtained from remote radiation measurements. J. Atmos. Sci., 29, 1262-1271.

Hamming, R.W., 1973: Numerical Methods for Scientists and Engineers. 2nd Edition, McGraw-Hill, New York, 721 pp.

King, J.I.F., 1985: Theory and application of differential inversion to remote temperature sensing. In Advances in Remote Sensing Retrieval Methods, A. Deepak, H.E. Fleming and M.T. Chahine (Eds.), Deepak Publishing Co., New York, 437-444.

Lacis, A.A., W.C. Wang and J.E. Hansen, 1979: Correlated k-distribution method for radiative transfer in climate models: Application to effect of cirrus clouds on climate. Fourth NASA Weather and Climate Program Science Review, 309-314.

Liou, K.N., 1980: An Introduction to Atmospheric Radiation. Academic Press, New York, 404 pp.

Liou, K.N., S.S. Ou and J.I.F. King, 1988: On the differential inversion method for temperature retrievals. In Remote Sensing Retrieval Methods, Deepak Publishing Co., New York (in press).

McClatchey, R.A., R.W. Fenn, J.E.A. Selby, F.E. Volz and J.G. Garing, 1971: Optical properties of the atmosphere. Environ Res. Pap. No. 354, AFCRL-71-0279 AD726116.

Pearson, C.E., 1974: Handbook of Applied Mathematics. Van Nostrand Reinhold Co., New York, 87-89.

Rothman, L.S., R.R. Gamache, A. Barbe, A. Goldman, J.R. Gillis, L.R. Brown, R.A. Toth, J.M. Flaud and C. Camy-Peyret, 1983: AFGL atmospheric line parameters compilation: 1982 edition. Appl. Opt., 22, 2247-2256.

Smith, W.L., 1970: Iterative solution of the radiative transfer equation for the temperature and absorbing gas profiles of an atmosphere. Appl. Opt., 9, 1993-1999.

Smith, W.L. et al., 1975: The high resolution infrared radiation sounder (HIRS) experiment. In Nimbus-6 User's Guide, NASA Goddard Space Flight Center, Hampton, VA, 37-58.

Twomey, S., 1963: On the numerical solution of Fredholm integral equations of the first kind by the inversion of the linear system produced by quadrature. J. Ass. Comput. Mach., 10, 97-101.

Widder, D.V., 1971: An Introduction to Transform Theory. Academic Press, New York, 253 pp.